Tripling Light Conversion Efficiency of μLED Displays by Light Recycling Black Matrix

Xiang Zhang, Anlan Chen, Tao Yang, Junhu Cai, Yuanyuan Ye, Enguo Chen, Sheng Xu, Yun Ye, Jie Sun, *Senior Member, IEEE*, Qun Yan, and Tailiang Guo

***Abstract*—Quantum-dot color conversion film (QDCCF) with a partitioned black matrix (BM) realizes effective color generation with low crosstalk for micro-light-emitting diode (μLED) displays. However, this traditional BM seriously deteriorates light conversion efficiency (LCE) of QD converted μLED displays due to its absorption energy loss. In this paper, a novel internal and external reflective black matrix (IERBM) is proposed to improve the LCE and blue light utilization (BLU) by light recycling and reuse. Based on the IERBM structural optimization, the LCE can be respectively improved by 3.39× and 2.74× for red and green QDCC sub-pixels, and the BLU can be effectively increased by 1.11×. Accurate white balance and high color uniformity are achieved by this μLED display. Meanwhile, both the crosstalk of 1.72% and the color gamut of 89.8% Rec. 2020 are comparable with traditional absorptive BM. It is also found that the proposed IERBM has the potential to weaken μLED's sidewall effect. This work may open up a new technological route for improving the optical performance in advanced self-emissive displays.**

***Index Terms*—Displays, quantum dots, micro LED, black matrix.**

I. Introduction

COLOR conversion is a dominating technique for realizing full-color displays [1]–[3]. For liquid crystal displays, white light from the backlight is firstly generated by blue LEDs and the capped yellow phosphors, and then three primary colors are separated by an absorptive color filter [4]–[6]. The combination of phosphors and color filter inevitably brings narrow color gamut and low optical efficiency, which is antithetical to the requirements of next-generation displays [7], [8]. As a potential game changer, quantum dots (QDs) have become a new research hotspot, which show the advantages of high efficiency, wide color gamut, satisfactory optical purity, adjustable color spectrum, and so on [9]–[13]. Currently, the QD enhanced film has gradually become mature for LCD backlights due to its unique photoluminescence characteristic and structural compatibility [13]–[16]. For self-luminous displays, such as organic light-emitting diode (OLED) or micro-light-emitting diode (μLED), the QDs can be patterned and pixelated as a color conversion layer aligned with excitation sub-pixels to improve the efficiency and color gamut [17], [18].

Ultra-high pixel density is a major milestone for advanced display technologies. μLED is a typical case, where a millimeter-level LED pixel is miniaturized into 100 microns [19]–[22]. Although μLED is considered as a disruptive technology in up-to-date displays [23], [24], it is not yet mature and still faces certain challenges, such as mass transfer [25], color formation [26], sidewall effect [27]–[29], and instable red luminescence [30]. Quantum-dot color conversion (QDCC) has been generally recognized as a promising color formation approach for μLED displays, because the nano-scale QD particles have higher photoluminescence quantum yields (PLQY) and better light uniformity than other fluorescent materials [31]–[34]. However, relatively low light conversion efficiency (*LCE*) is still a problem for QD converted μLED displays.

By summarizing existing literatures, the *LCE* improving methods for QD converted μLED displays can be classified into three aspects, including raw material modification, auxiliary color conversion structure, and light collection approach. By using QD material modification, the *LCE* of the LEDs can be enhanced to 32.4% by embedding nanorods into microholes [35]. Another example is introducing perovskite QDs (PQDs) with a higher PLQY into LEDs [36]. As an auxiliary color conversion structure, hybrid and distributed Bragg reflectors were inserted in μLED displays, which could increase the red and green light output intensity by 27%. [37]. In terms of light collection approach, a funnel-tube structural array designed on color-converted μLEDs was proved to be effective for both light efficiency promotion and crosstalk elimination [38]. An epoxy lens encapsulated on a blue μLED can increase the efficiency by 129% to the maximum extent [39]. Although diverse methods have been developed for improving *LCE* and blue light utilization (*BLU*) for μLED displays, few researches have paid

Manuscript received November 30, 2021; revised January 25, 2022; accepted January 28, 2022. Date of publication February 4, 2022; date of current version February 14, 2022. This work was supported in part by the National Natural Science Foundation of China under Grant 62175032, in part by Fujian Provincial Natural Science Foundation Project under Grant 2021J01579, in part by Fujian Provincial Key Science and Technology Project under Grant 2021HZ021001, and in part by the Fujian Science & Technology Innovation Laboratory for Optoelectronic Information of China under Grant 2020ZZ111. *(Corresponding author: Enguo Chen.)*

Xiang Zhang, Anlan Chen, Tao Yang, Junhu Cai, and Yuanyuan Ye are with the National & Local United Engineer Laboratory of Flat Panel Display Technology, College of Physics and Information Engineering, Fuzhou University, Xueyuan Road Fuzhou, Fujian Province 350108, China (e-mail: 1035032492@qq.com; 1157426235@qq.com; 645492022@qq.com; 976162336@qq.com; 945846609@qq.com).

Enguo Chen, Sheng Xu, Yun Ye, Jie Sun, Qun Yan, and Tailiang Guo are with the National & Local United Engineer Laboratory of Flat Panel Display Technology, College of Physics and Information Engineering, Fuzhou University, Xueyuan Road Fuzhou, Fujian Province 350108, China, and also with the Fujian Science & Technology Innovation Laboratory for Optoelectronic Information of China, Fuzhou, Fujian 350108, China (e-mail: ceg@fzu.edu.cn; xusheng06090@163.com; yeyun07@fzu.edu.cn; jie.sun@chalmers.se; qunfyan@gmail.com; gtl_fzu@hotmail.com).

Digital Object Identifier 10.1109/JPHOT.2022.3148241

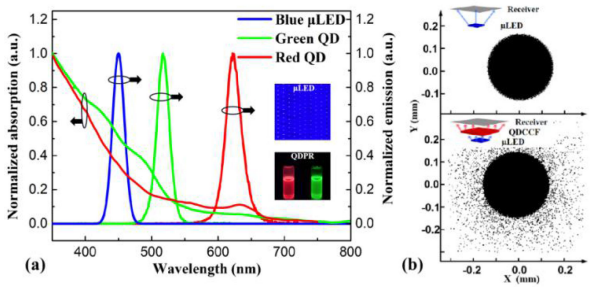

Fig. 1. (a) Absorption and emission spectra of red and green QDs and the emission spectrum of μLED array; (b) Scattering property of a bare μLED and a QD converted μLED.

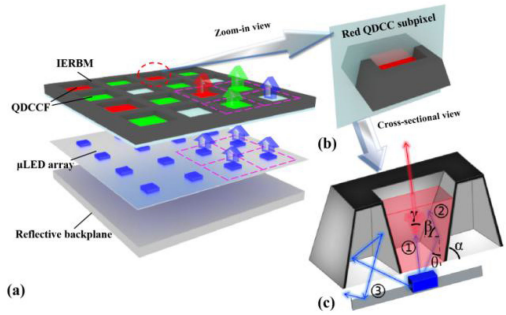

Fig. 2. (a) Schematic for QD-converted μLED display architecture based on the IERBM; (b) Zoom-in view of a single red sub-pixel with the surrounding IERBM; (c) Three representative light paths inside the IERBM.

attention to the black matrix itself on the QDCC film (QDCCF), which is responsible for the most serious absorption loss in displays.

The black matrix (BM) is indispensable for QD converted μLEDs. It is used to isolate the three-primary-color QD sub-pixels, so as to prevent color crosstalk and enhance contrast ratio of μLED displays [40], [41]. A traditional BM, made by black photoresist material, can absorb most of light incident to the BM's surface [42], [43]. This absorbed light energy accounts for a large proportion of μLED's emission, because the wide angular distribution of μLED displays comes from both the lambertian intensity distribution of μLED and the QD's isotropic scattering [44], [45]. It is obvious that this absorptive BM will tremendously affect the light output and deteriorate the *LCE* of QD converted μLEDs. There still exists a research gap to recycle or reuse the light energy absorbed by the traditional BM, which is of great practical significance for *LCE* improvement of μLED displays.

This paper aims to propose a simple but effective architecture, wherein a novel black matrix with internal and external reflective interfaces (abbreviated as IERBM) is presented to dramatically improve the *LCE* and *BLU* in QD converted μLED displays. The design principle of this IERBM is described to find an optimal structure for light recycling and reuse. Moreover, key performance of this IERBM is verified and compared with traditional absorptive BM structure and other potential BM structures.

II. Theoretical Model

A. Fundamentals

For color converted μLED displays, the blue μLED array is used as excitation sources, and the upper QDCCF is patterned and pixelated into isolated sub-pixels that separate red and green QDs. A blue sub-pixel contains scattering particles without any QDs. The blue μLED array is aligned with the QDCC sub-pixels, and the QD sub-pixels will have complex optical responses to the excitation blue light, including absorption, emission, and scattering [3], [46].

As shown in Fig. 1(a), the absorption and emission spectra of red and green QDs were respectively tested by F-4600 (Hitachi, Ltd) and UV-3600 (Shimadzu, Ltd), and fitted by Gaussian Function. The QD's scattering property was characterized via simulation, which is drawn in Fig. 1(b). The inset pictures of Fig. 1(b) show the light path of a bare μLED and a QD converted μLED. Meanwhile, the corresponding footprints of the unconverted and converted light on the receiving plate are recorded in the *xy* coordinate system, respectively. It can be seen from the upper picture of Fig. 1(b) that the light spot is highly concentrated without a QDCCF, but is enlarged obviously with an inserted QDCCF (seen in the lower picture of Fig. 1(b)). This phenomenon proves the strong isotropic scattering caused by the QDCCF, which is the main cause for the absorption loss of a traditional BM.

B. Design Principle of The IERBM

It is hard to confine the converted light inside a sub-pixel range due to the QD scattering, and the spread light may cause unwanted crosstalk and deteriorate the *LCE*. As shown in Fig. 2, the IERBM is proposed to address this issue, which has funnel-shaped edges, internal hollow structure, and a tetrahedral aperture. Fig. 2(a) illustrates the double-layered QD-converted μLED display architecture. The μLED backplane is placed at the bottom of the QDCCF, and there has a one-to-one correspondence between a single μLED pixel and a QD sub-pixel. The QD sub-pixels are isolated by the IERBM shown in Fig. 2(b). Reflective coating is set on the internal and external interfaces of the IERBM, which helps to recycle and reuse the incident light instead of absorption loss. Fig. 2(c) draws three representative light paths inside the IERBM. Light path ① represents that the blue light is emitted from μLED and then converted into red light. After QD scattering, part of the converted red light directly passes through the QDCCF. Light path ② is the external reflection of the light by the IERBM, which increases the chance of the QD excitation by the unconverted blue light. As for light path ③, the light emitted from the μLED with a large spread angle will also be internally reflected and recycled after the backplane's reflection. It is noted that the gray layers in Fig. 2(c) represent the reflective coating surfaces, while the black layers represent the absorptive ones that prevent direct reflection of ambient light. It can be seen that the light recycling and reuse of μLEDs can be realized by using the IERBM structure.

Considering the light paths inside the IERBM, the QD's scattering intensity of an arbitrary position can be expressed

by using Mie theory [47]:

$$I_{sca} = I_0 \frac{\lambda^2}{8\pi^2 d^2} I(\gamma) \tag{1}$$

$$I(\gamma) = A^2 |S_1(\gamma)|^2 + \left(1 - A^2\right) |S_2(\gamma)|^2 \tag{2}$$

where λ denotes the incident light wavelength, I_0 represents the intensity of incident light, I_{sca} represents the intensity of the scattering light, γ is the scattering angle (deflection angle relative to the vertical direction), d is the distance to the scattering particles. A is a directional parameter related to μLED's emitting light. $S(\gamma)$ is described as an amplitude function related to γ. As mentioned above, the scattering angle γ varies slightly, so that I_{sca} is limited within a small angle.

As shown in Figs. 1(b) and 2(c), the outgoing direction of the converted light is largely determined by the μLED's emitting angle, and the QD scattering also has non-negligible impact on the light spread angle. Therefore, the external reflection angle β on the IERBM's interface can be derived by law of reflection, which is determined by the tilt angle α of the IERBM.

$$\beta = \frac{3}{2} k\pi - [(2k-1)\alpha + (\theta \pm \gamma)] \tag{3}$$

where θ denotes the angle between certain designated light and the vertical direction, k is an index representing number of reflections. It is obvious that α has larger impact on β when $k > 1$ and has similar effect with θ when $k = 1$. Moreover, k becomes larger with a decreasing β due to the relative reflection between two opposite interfaces of the IERBM. As a key parameter of the IERBM, α will be further discussed in the following section.

C. Performance Indicators

The QD converted light is partially absorbed and scattered during the propagation process, so that the intensity of the converted light is not equal to that of the actual output light. As a performance indicator for the IERBM, *LCE* can be defined as the ratio of the intensity of the actual converted light (I_{con}) and the total intensity of the blue light incident into the QDCCF (I_{in}) [48]:

$$LCE = \frac{I_{con}}{I_{in}} \tag{4}$$

Blue light utilization rate (*BLUR*) is another important performance indicator for the IERBM, which can be defined as the ratio of I_{in} and the total intensity of the light emitted from μLED ($I_{\mu LED}$):

$$U = \frac{I_{in}}{I_{\mu LED}} \tag{5}$$

where, U is the *BLUR* of the proposed IERBM.

In order to compare the IERBM with the traditional absorptive BM, an indicator, δ_U, is defined to evaluate the utilization changing rate:

$$\delta_U = \frac{U - U_{tBM}}{U} \tag{6}$$

where U_{tBM} is the *BLUR* of the traditional absorptive BM.

As Shown in Fig. 2(b), the Relative Aperture Size of the IERBM and QDCCF Can Be Expressed By

$$r = \frac{L_b}{L_q} \tag{7}$$

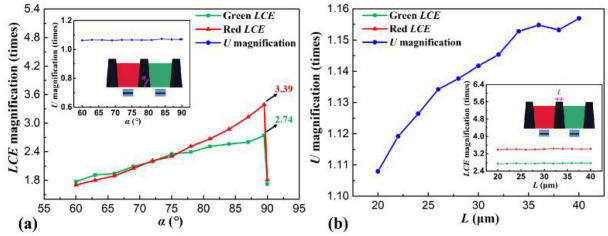

Fig. 3. Simulation results of the IERBM based on different tilt angles α (a) and top side length L (b).

where L_b and L_q are the top side length of the IERBM and the QDCCF, respectively.

Once the QDs' population density and the film-forming materials are selected, the parameters of I_{in}, $I_{\mu LED}$, and I_{con} can be determined, so that the parameters of *LCE*, U, and δ_U can be further obtained by the actual intensity.

III. Simulation Results

A. Light Conversion Efficiency (LCE) and Blue Light Utilization (BLU)

As shown in Fig. 3, two parameters of the IERBM, tilt angle α and top side length L, were optimized while the thickness of IERBMs and QDCCFs was 15 μm and 10 μm, respectively. Only one of the two parameters was changed during each simulation. The absorption and emission spectra in Fig. 1(a) were used for simulating red/green QDCCFs and blue μLEDs. The red/green QDs in the sub-pixels have the size of 4.5 nm and 5.5 nm, respectively. In addition, the scattering particles of TiO_2 with the size of 200 nm were distributed in the blue sub-pixels, following Mie theory. Simulation results show that when the thickness of QDCCF is set to 10 μm, the blue light transmission can be significantly reduced to lower than 0.1%.

Fig. 3 shows the simulation results of *LCE* magnification and *U* magnification of the IERBM. It is noted that the *LCE* magnification here reflects the ratio of the normalized *LCE* between the IERBM and the traditional absorptive BM. In Fig. 3(a), the tilt angle varied from 60° to 90°, while the top side length was set to be 20 μm. In Fig. 3(b), the top side length ranged from 20 μm to 40 μm when the tilt angle was fixed at 89.5°. The μLED's size is set to 20 μm × 20 μm, and there is an air gap of 30 μm between the μLED and IERBM structure.

From these curves, the *LCE* magnification increases as the tilt angle increases, and it remains stable when the top side length increases. On the contrary, the fluctuation of *U* magnification is quite small when the tilt angle changes from 60° to 90°, but *U* magnification becomes larger with the increase of the top side length.

Smaller β means the increasing number of light reflections on the interfaces of the IERBM. Since the thicknesses of the QDCCFs and IERBMs are pre-determined, more times of reflections on the inner interfaces mean more opportunities of QDs' emission by the incident blue light. Therefore, a large amount of unconverted light can be recycled to improve the *LCE* due to multiple reflections. In Fig. 3(a), the *LCE* magnification of the red sub-pixels is 3.39× higher than the traditional absorptive BM, and the *LCE* magnification of the green sub-pixels also reaches 2.74× approaching triples. However, the *LCE* magnification

TABLE I
LCE MAGNIFICATION AND U MAGNIFICATION OF DIFFERENT IERBMS FOR RED QDCC SUB-PIXELS

IERBM (α, L)	I (75°, 20)	II (75°, 30)	III (90°, 30)	IV (89.5°, 20)
LCE magnification	2.31×	2.30×	1.82×	3.39×
U magnification	1.07×	1.14×	1.14×	1.11×

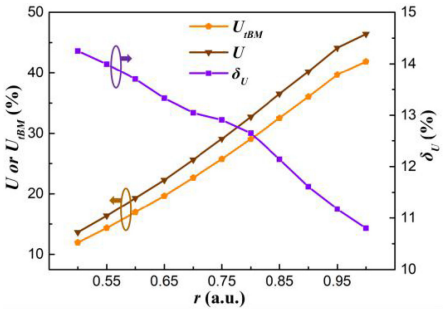

Fig. 4. Simulation results of the *BLUR* of the IERBM (U), the *BLUR* of the traditional absorptive IERBM (U_{tBM}), and the utilization changing rate (δ_U).

decreases sharply when $\alpha = 90^{\circ}$. Actually, the sharp drop of the *LCE* magnification only occurs at $\alpha = 90^{\circ}$, which comes from the IERBM structure with regular-shaped edges. That is because most of incident light oscillates repeatedly within the IERBM. In this case, the IERBM is like a cavity, in which the light will be reflected by the sidewall many times until absorption loss. In Fig. 3(b), the *LCE* magnification keeps stable, which means that the incident light entering the QDCCFs is almost constant when the light distribution of μLED is determined.

In Table I, four different IERBMs with the red QDCC sub-pixel are compared. They are differentiated by the parameters of tilt angle α and top side length L, and labelled by I ($\alpha = 75^{\circ}$, $L = 20$μm), II ($\alpha = 75^{\circ}$, $L = 30$μm), III ($\alpha = 90^{\circ}$, $L = 30$μm), and IV ($\alpha = 89.5^{\circ}$, $L = 20$μm). The *LCE* magnification and U magnification of these four IERBMs are listed in Table I. Compared with a traditional absorptive BM, the *LCE* magnification and U magnification of the IERBM are improved in varying degrees, indicating higher optical performance. Specifically, the *LCE* enhancement of IERBM IV reaches 3.39× of a traditional absorptive BM. U magnification is stable from Table I, since it is significantly affected by L.

The utilization between the traditional absorptive BM and the IERBM was compared by changing the relative size of the BM and QDCCF. As shown in Fig. 4, U_{tBM} and U decrease obviously with the decline of r. On the contrary, a negative relationship is found between δ_U and r, suggesting that the IERBMs have a better effect on utilization improvement with a lower r.

B. White Balance Realization

The IERBM with $\alpha = 89.5^{\circ}$ and $L = 20$ μm is used for further discussion. A white-balanced QDCCF commonly contains separate three-primary-color or multi-primary-color sub-pixels that are aligned with the bottom blue μLED array [17], [49]. The

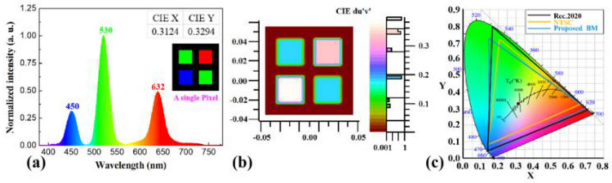

Fig. 5. (a) White balance spectrum, (b) color uniformity diagram, (c) color gamut and the white point of the QD converted μLED employing the IERBM.

TABLE II
THE PARTICLE POPULATION DENSITIES FOR WHITE BALANCE

Particles	Red sub-pixels	Green sub-pixels	Blue sub-pixels
QDs	4.62×10^{14}/mm^3	2.19×10^{14}/mm^3	None
TiO_2	1.67×10^{9}/mm^3	1.65×10^{9}/mm^3	2.74×10^{10}/mm^3

results in Fig. 3(a) have shown that the *LCE* magnification of green QDCC sub-pixels is much lower than red. That means the proportion of green sub-pixels should be enlarged to compensate the low *LCE* for white balance. Therefore, a single QDCC pixel herein is composed of four sub-pixels, including one red sub-pixel, two identical green sub-pixels, and one blue sub-pixel. The four QDCC sub-pixels, isolated by the IERBMs, were established and simulated. The simulated white-balanced spectrum is shown in Fig. 5(a). By changing the QDs' particle population density, the Commission Internationale de l'Eclairage (CIE) coordinates are finally obtained as (0.3124, 0.3294) for white balance.

The white balance was achieved by adjusting different particle population densities. The final particle population densities of red / green QDs and TiO_2 particles are listed in Table II. The color uniformity diagram of this QD converted μLED is shown in Fig. 5(b), indicating that high color uniformity can be obtained by the IERBM. The color uniformity (du' dv') can be calculated under CIE 1976 color space as the following equation:

$$du'dv' = \sqrt{(u' - u_{ref}')^2 + (v' - v_{ref}')^2} \tag{8}$$

where (u', v') is the actual chromaticity coordinates in CIE 1976, and (u_{ref}, v_{ref}) represents the chromaticity coordinates for the chosen reference color. Here, the standard white point is selected as the reference. After calculation, the chromatic aberration of all sub-pixels is highly consistent within an offset lower than 0.005, which exhibits excellent color uniformity. Moreover, as shown in Fig. 5(c), the color gamut covers 89.8% Rec. 2020 standard and 120.6% NTSC, showing high color purity for the μLED displays.

It is worth mentioning that emitting peaks caused by crosstalk can be well filtered by traditional absorptive color filters [50]. Here, both the calculation of color coordinates and the corresponding color gamut only considers the QDs' primary emission peak and the μLED's emission wavelength.

Angular color shift performance can be evaluated by the spatial light intensity distribution of the trichromatic sub-pixels. Simulation results in Fig. 6 show that the spatial light intensity

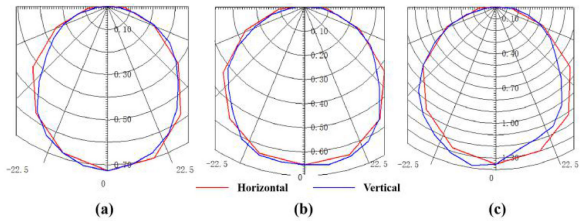

Fig. 6. The spatial light intensity distribution of the blue sub-pixel (a), the red sub-pixel (b) and the green sub-pixel (c).

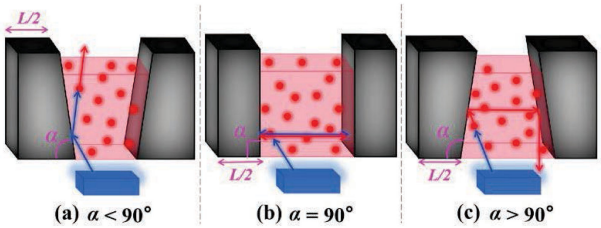

Fig. 7. (a) The proposed IERBM with funnel-shaped edges ($\alpha < 90^{\circ}$); (b) The potential IERBM with regular-shaped edges ($\alpha = 90^{\circ}$); (c) The potential IERBM with inverted funnel-shaped edges ($\alpha > 90^{\circ}$).

distribution of the trichromatic sub-pixels is quite similar due to the scattering effect of QDs and scattering particles. It means that the angular color shift performance should be acceptable for this structure.

IV. Discussion and Analysis

A. Comparisons Among Different IERBM Structures

Here, the proposed IERBM structure and other two potential IERBM structures are compared, including the proposed IERBM with funnel-shaped edges ($\alpha < 90^{\circ}$), the potential IERBM with regular-shaped edges ($\alpha = 90^{\circ}$), and the potential IERBM with inverted funnel-shaped edges ($\alpha > 90^{\circ}$). Among these structures, the proposed IERBM is the most suitable for light extraction and *LCE* improvement, which can be seen in the light path shown in Fig. 7(a). If the IERBM is built by the regular-shaped edges shown in Fig. 7(b), the light will oscillate repeatedly inside the QDCCF, resulting in serious energy loss. By using the IERBM in Fig. 7(c), most of the light will be trapped inside due to the reflection direction of the opposite interfaces.

For further verification, a receiver is inserted between the QDCCF and the corresponding μLED to detect the reflected light and incident light. The converted light reflecting back to the μLED's backplane is defined as R_f, which can be calculated as:

$$R_f = \frac{I_{back}}{I_{in}} \tag{9}$$

where I_{back} is the intensity of the converted light that is reflected back to the μLED's backplane.

Comparison results of three structures are listed in Table III. Here, R_f is normalized to the proposed IERBM shown in Fig. 7(a), so that R_f of the first column is 1.00. R_f of the third column is obviously higher than the other two columns, which means a high energy loss due to the reflective light back to the μLED's backplane. This reveals that the third IERBM is not applicable for μLED displays. In the second row of Table III, the *LCE* magnification of the proposed IERBM is significantly larger than that in the second column. These results demonstrate the proposed IERBM ($\alpha < 90^{\circ}$) is the best structure to achieve *LCE* gains.

TABLE III
Comparisons of Three Potential IERBM Structures in Fig. 7

	IERBM structure in Fig. 7(a) ($\alpha <$ 90°)	IERBM structure in Fig. 7(b) ($\alpha =$ 90°)	IERBM structure in Fig. 7(c) ($\alpha >$ 90°)
R_f	1.00	0.96	1.15
LCE magnification	3.39×	1.81×	Not Applicable

B. Discussion on Performance Improvement of the IERBM

The basic reason of the *LCE* improvement by IERBM can be summarized as the internal and external interface coating with reflective films. By this structure, the color gamut can be kept at the same level as the traditional absorptive BM without sacrificing the *LCE*.

Here, crosstalk is taken into consideration as another important performance indicator. It reflects the leaking light from neighboring sub-pixels. The crosstalk's definition can be expressed as the ratio of the leakage intensity $I_{leakage}$ to the target sub-pixel and the total light intensity of this target sub-pixel I_{total}:

$$R_c = \frac{I_{leakage}}{I_{total}} = \frac{I_{total} - I_{sub-pixel}}{I_{total}} \tag{10}$$

where R_c is the crosstalk level of the target sub-pixel, $I_{sub\text{-}pixel}$ is the intensity from the target sub-pixel itself.

Due to the reflective structure of the IERBM, the ambient light may have a higher reflection than the traditional BM. Here, the ambient reflection rate R_a is defined for comparison:

$$Ra = \frac{Ic}{Ia} \tag{11}$$

where, I_c is the intensity of the conversion light under ambient light excitation, I_a is the intensity of the ambient light.

As shown in Table IV, the *LCE* magnification and *U* magnification of the red and green QDCCFs show a great improvement compared with the traditional absorptive BM. At the same time, the crosstalk of the IERBM is kept at the same level as the traditional absorptive BM, which could hardly affect the display effect.

In Table IV, it is worth noting that the *LCE* magnification of the red and green QDCCFs is not balanced because of the difference of their absorption spectra. As shown in Fig. 1(a), red QDs have weaker absorption at 450 nm than green. However, it can be found that the self-absorption at green band is almost double of red. This is the primary reason that the *LCE* magnification of red QDs is able to be higher than green.

TABLE IV
COMPARISONS OF THE KEY PERFORMANCE BETWEEN THE TRADITIONAL ABSORPTIVE BM AND THE PROPOSED IERBM

	Key performance					
	R-LCE magnification	*G-LCE* magnification	R-R_a	G-R_a	*U* magnification	R_c
Traditional absorptive BM	1.00×	1.00×	9.57%	8.65%	1.00×	0.12%
IERBM	3.39×	2.74×	21.87%	16.78%	1.11×	1.72%

It can be seen in Table IV that R_a of the proposed IERBM is almost 2× larger than the traditional absorptive BM, which brings the brightness improvement of the display panel. Unfortunately, this could in turn reduce the ambient contrast of this displays. To solve this problem, the traditional absorptive color filters can be added above the QDCCF to reduce the effect of ambient light on this display structure. By adding traditional absorptive color filters, the simulated ambient reflection rate can be reduced to 2.08% and 2.68% for red and green sub-pixels, respectively.

C. Reduced Sidewall Effect of μLED Displays

As is known, the sidewall effect becomes more serious with the size shrinkage of μLEDs, resulting in the decline of the light utilization. This has become a potential bottleneck problem for μLED displays. A possible solution found in existing literatures is the internal optimization of μLED's laminated structure [51], [52].

Based on law of energy conservation, the emitting light with a wide spread angle increases with the area of the μLED's side wall, which will largely be absorbed by traditional BM and result in serious light loss. By using the IERBM, this part of light will be guided into the internal reflection structure, and reflected back to the μLED backplane, as illustrated in light path ③ in Fig. 2(c). This part of light will be recycled and incident into the QDCCF again through the diffuse reflection of the μLED backplane. Even though the multiple light reflection and diffusion will cause some energy loss, the sidewall effect can be reduced to some extent by the proposed IERBM, and this would become much more obvious with smaller μLEDs.

Due to the sidewall effect, the simulation results show that the reflection path does cause certain crosstalk increase, but in fact, the recycling light is much more than the light causing crosstalk [38]. Although the sidewall effect increases the light emitting from the sidewall, the vast majority of such crosstalk comes from the light with ultra large angle, which only occupies a very limited percentage of total emission. In order to reduce the crosstalk, the air gap between μLED and QDCCF should be set small enough, or we can add certain damming structure between neighboring sub-pixels.

D. Potential Preparation Methods

Potentially feasible preparation methods are discussed to obtain the proposed IERBM structure. The vacuum vapor deposition could be used here on a pre-prepared inverted funnel-shaped mask after internal formation by nanolithography to shape the basic structure. And after that, a silver coating can be used on the structure's surface by means of atomic layer deposition. For alternative, three-dimensional mold pouring is also a potential method for IERBM molding. A hollow template of the required shape is firstly prepared and then filled with the molding material.

Since the proposed IERBM has over tens of micron level, current micro or nano processing technique can well satisfy the fabrication requirement of the IERBM, which provides the processing accuracy below 100 nm and the angular accuracy below 0.1°. For example, the nanostructured processes, such as nano-gratings [53] and nano-printing [54], are appropriate for this. The inner and outer prismatic structures can be prepared by nanoimprinting, and then the inner and outer slanted edges are further processed by using ion beam etching. Compared with the aforementioned two methods, it is more advantageous in processing micro and nano structures.

The above are several potential methods that could guide the actual processing of the proposed IERBM. Although these methods have their own unique merits and drawbacks, it is expected to see one or more potential preparation methods to obtain the proposed IERBM in the near future.

V. CONCLUSION

Shrinkage in pixel size from conventional LED into μLED brings about dramatic decrease of light conversion efficiency (*LCE*). Existing *LCE* improvement approaches mainly focus on the QDCCF and μLED structures, whereas the black matrix has not been taken into consideration yet. In this paper, we propose an internal and external reflective black matrix (IERBM) to achieve higher *LCE* and *BLU* of QD-based μLED displays. By optimizing the tilt angle and top side length of the IERBM, the *LCE* can be increased by 3.39× with the proposed IERBM, and the *BLU* magnification finally reaches 1.11×. Meanwhile, both the crosstalk of 1.72% and the color gamut of 89.8% Rec. 2020 are comparable with traditional absorptive BM. White balance with CIE coordinates of (0.3124, 0.3294) can be achieved with high color uniformity. The proposed IERBM is also applicable to other kinds of color conversion layers for *LCE* improvement, such as phosphors, organic conversion material. It is expected that the IERBM may open up a new technological route to improve luminous efficiency of other advanced self-emissive displays.

REFERENCES

[1] G. Kim, Y. Shih, and F. G. Shi, "Optimal design of a quantum dot color conversion film in LCD backlighting," *IEEE J. Sel. Topics Quantum Electron.*, vol. 23, no. 5, Sep./Oct. 2017, Art. no. 4800404.
[2] R. Tangirala *et al.*, "86-2: Color conversion using quantum dots for LCD, OLED, and MicroLED displays," *SID Symp. Dig. Tech. Papers*, vol. 51, no. 1, pp. 1299–1302, 2020.
[3] H. Chen, J. He, and S. Wu, "Recent advances on quantum-dot-enhanced liquid-crystal displays," *IEEE J. Sel. Topics Quantum Electron.*, vol. 23, no. 5, Sep./Oct. 2017, Art. no. 1900611.

[4] J. K. Park, H. K. Chang, S. H. Park, H. D. Park, and S. Y. Choi, "Application of strontium silicate yellow phosphor for white light-emitting diodes," *Appl. Phys. Lett.*, vol. 84, no. 10, pp. 1647–1649, 2004.

[5] N. T. Tran, J. P. You, and F. G. Shi, "Effect of phosphor particle size on luminous efficacy of phosphor-converted white LED," *J. Lightw. Technol.*, vol. 27, no. 22, pp. 5145–5150, 2009.

[6] Y. Ito *et al.*, "59.1: A backlight system with a phosphor sheet providing both wider color gamut and higher efficiency," *SID Symp. Dig. Tech. Papers*, vol. 44, no. 1, pp. 816–819, 2013.

[7] G. R. Fern, P. G. Harris, T. G. Ireland, and J. Silver, "P-121: Sub-micrometre phosphor preparation for next generation displays," *SID Symp. Dig. Tech. Papers*, vol. 48, no. 1, pp. 1711–1714, 2017.

[8] T. Takeda, N. Hirosaki, S. Funahshi, and R.-J. Xie, "Narrow-band green-emitting phosphor $Ba_2LiSi_7AlN_{12}$:Eu^{2+} with high thermal stability discovered by a single particle diagnosis approach," *Chem. Mater.*, vol. 27, no. 17, pp. 5892–5898, 2015.

[9] R. Zhu, Z. Luo, H. Chen, Y. Dong, and S. T. Wu, "Realizing rec. 2020 color gamut with quantum dot displays," *Opt. Exp.*, vol. 23, no. 18, pp. 23680–23693, 2015.

[10] Y. Shirasaki, G. J. Supran, M. G. Bawendi, and V. Bulović, "Emergence of colloidal quantum-dot light-emitting technologies," *Nature Photon.*, vol. 7, no. 1, pp. 13–23, 2013.

[11] Y.-H. Ko, M. Jalalah, S.-J. Lee, and J.-G. Park, "Super ultra-high resolution liquid-crystal-display using perovskite quantum-dot functional color-filters," *Sci. Reps.*, vol. 8, no. 1, pp. 1–7, 2018.

[12] Y. Shih and F. G. Shi, "Quantum dot based enhancement or elimination of color filters for liquid crystal display," *IEEE J. Sel. Topics Quantum Electron.*, vol. 23, no. 5, Sep./Oct. 2017, Art. no. 1901304.

[13] E. Chen *et al.*, "Flexible/curved backlight module with quantum-dots microstructure array for liquid crystal displays," *Opt. Exp.*, vol. 26, no. 3, pp. 3466–3482, 2018.

[14] E. Jang, S. Jun, H. Jang, J. Lim, B. Kim, and Y. Kim, "White-light-emitting diodes with quantum dot color converters for display backlights," *Adv. Mater.*, vol. 22, no. 28, pp. 3076–3080, 2010.

[15] Z. Luo, Y. Chen, and S.-T. Wu, "Wide color gamut LCD with a quantum dot backlight," *Opt. Exp.*, vol. 21, no. 22, pp. 26269–26284, 2013.

[16] H. C. Yoon, H. Lee, H. Kang, J. H. Oh, and Y. R. Do, "Highly efficient wide-color-gamut QD-emissive LCDs using red and green perovskite core/shell QDs," *J. Mater. Chem. C*, vol. 6, no. 47, pp. 13023–13033, 2018.

[17] E. Chen *et al.*, "Asymmetric quantum-dot pixelation for color-converted white balance," *ACS Photon.*, vol. 8, no. 7, pp. 2158–2165, 2021.

[18] S. Xu *et al.*, "Precise theoretical model for quantum-dot color conversion," *Opt. Exp.*, vol. 29, no. 12, pp. 18671–18685, 2021.

[19] S. X. Jin, J. Li, J. Z. Li, J. Y. Lin, and H. X. Jiang, "GaN microdisk light emitting diodes," *Appl. Phys. Lett.*, vol. 76, no. 5, pp. 631–633, 2000.

[20] H. X. Jiang and J. Y. Lin, "Nitride micro-LEDs and beyond-a decade progress review," *Opt. Exp.*, vol. 21, no. S3, pp. A475–A484, 2013.

[21] Z. Liu, W. C. Chong, K. M. Wong, and K. M. Lau, "GaN-based LED micro-displays for wearable applications," *Microelectronic Eng.*, vol. 148, pp. 98–103, 2015.

[22] G. Tan, Y. Huang, M.-C. Li, S.-L. Lee, and S.-T. Wu, "High dynamic range liquid crystal displays with a mini-LED backlight," *Opt. Exp.*, vol. 26, no. 13, pp. 16572–16584, 2018.

[23] T. Wu *et al.*, "Mini-LED and micro-led: Promising candidates for the next generation display technology," *Appl. Sci.*, vol. 8, 2018, Art. no. 1557.

[24] H.-V. Han *et al.*, "Resonant-enhanced full-color emission of quantum-dot-based micro LED display technology," *Opt. Exp.*, vol. 23, no. 25, pp. 32504–32515, 2015.

[25] X. Zhou *et al.*, "Growth, transfer printing and colour conversion techniques towards full-colour micro-LED display," *Prog. Quantum Electron.*, vol. 71, 2020, Art. no. 100263.

[26] T. Wu, Y. M. Huang, J. S. Konthoujam, Z. Chen, and H. C. Kuo, "Quantum-dot-based full-color micro-LED displays," *Semiconductors Semimetals*, vol. 106, 2021, Art. no. 173-201.

[27] P. Tian *et al.*, "Size-dependent efficiency and efficiency droop of blue InGaN micro-light emitting diodes," *Appl. Phys. Lett.*, vol. 101, no. 23, 2012, Art. no. 231110.

[28] F. Olivier, A. Daami, C. Licitra, and F. Templier, "Shockley-Read-Hall and Auger non-radiative recombination in GaN based LEDs: A size effect study," *Appl. Phys. Lett.*, vol. 111, no. 2, 2017, Art. no. 022104.

[29] F. Gou *et al.*, "Angular color shift of micro-LED displays," *Opt. Exp.*, vol. 27, no. 12, pp. A746–A757, 2019.

[30] Z. Chen, S. Yan, and C. Danesh, "MicroLED technologies and applications: Characteristics, fabrication, progress, and challenges," *J. Phys. D: Appl. Phys.*, vol. 54, no. 12, 2021, Art. no. 123001.

[31] T.-H. Kim, S. Jun, K.-S. Cho, B. L. Choi, and E. Jang, "Bright and stable quantum dots and their applications in full-color displays," *MRS Bull.*, vol. 38, no. 9, pp. 712–720, 2013.

[32] X. Dai *et al.*, "Solution-processed, high-performance light-emitting diodes based on quantum dots," *Nature*, vol. 515, no. 7525, pp. 96–99, 2014.

[33] Z. Liu *et al.*, "Micro-light-emitting diodes with quantum dots in display technology," *Light: Sci. Appl.*, vol. 9, no. 1, 2020, Art. no. 83.

[34] E.-L. Hsiang, Z. He, Y. Huang, F. Gou, Y.-F. Lan, and S.-T. Wu, "Improving the power efficiency of micro-LED displays with optimized LED chip sizes," *Crystals*, vol. 10, no. 6, 2020, Art. no. 494.

[35] C.-Y. Liu *et al.*, "Color-conversion efficiency enhancement of quantum dots via selective area nano-rods light-emitting diodes," *Opt. Exp.*, vol. 24, no. 17, pp. 19978–19987, 2016.

[36] H.-C. Wang, Z. Bao, H.-Y. Tsai, A.-C. Tang, and R.-S. Liu, "Perovskite quantum dots and their application in light-emitting diodes," *Small*, vol. 14, no. 1, 2018, Art. no 1702433.

[37] G. Chen, B. Wei, C. Lee, and H. Lee, "Monolithic red/green/blue Micro-leds with HBR and DBR structures," *IEEE Photon. Technol. Lett.*, vol. 30, no. 3, pp. 262–265, Feb. 2018.

[38] F. Gou, E.-L. Hsiang, G. Tan, Y.-F. Lan, C.-Y. Tsai, and S.-T. Wu, "Tripling the optical efficiency of color-converted micro-LED displays with funnel-tube array," *Crystals*, vol. 9, no. 1, 2019, Art. no. 39.

[39] S. Lan, H. Wan, J. Zhao, and S. Zhou, "Light extraction analysis of AlGaInP based red and GaN based blue/green flip-chip micro-leds using the monte carlo ray tracing method," *Micromachines*, vol. 10, no. 12, 2019, Art. no. 860.

[40] H.-Y. Lin *et al.*, "Optical cross-talk reduction in a quantum-dot-based full-color micro-light-emitting-diode display by a lithographic-fabricated photoresist mold," *Photon. Res.*, vol. 5, no. 5, pp. 411–416, 2017.

[41] K. Zhang, D. Peng, W. C. Chong, K. M. Lau, and Z. Liu, "Investigation of photon-generated leakage current for high-performance active matrix Micro-LED displays," *IEEE Trans. Electron Devices*, vol. 63, no. 12, pp. 4832–4838, Dec. 2016.

[42] J. Choi *et al.*, "P-74: Synthesis and characterizations of high-photosensitive monomers for black matrix in liquid crystal displays," *SID Symp. Dig. Tech. Papers*, vol. 42, no. 1, pp. 1379–1381, 2011.

[43] L. Y. Kuo *et al.*, "P-167: Efficiency improvement of an organic light emitting display with black matrix for high contrast ratio," *SID Symp. Dig. Tech. Papers*, vol. 47, no. 1, pp. 1747–1749, 2016.

[44] Z. Li, J. Li, J. Li, Z. Deng, Y. Deng, and Y. Tang, "Scattering effect on optical performance of quantum dot white light-emitting diodes incorporating SiO_2 nanoparticles," *IEEE J. Quantum Electron.*, vol. 56, no. 3, Jun. 2020, Art. no. 3600109.

[45] C. Würth, D. Geißler, and U. Resch-Genger, "Quantification of anisotropy-related uncertainties in relative photoluminescence quantum yield measurements of nanomaterials – semiconductor quantum dots and rods," *Zeitschrift für Physikalische Chemie*, vol. 229, no. 1-2, pp. 153–165, 2015.

[46] Z. Du, M. Artemyev, J. Wang, and J. Tang, "Performance improvement strategies for quantum dot-sensitized solar cells: A review," *J. Mater. Chem. A*, vol. 7, no. 6, pp. 2464–2489, 2019.

[47] J. Xiang and J. He, "Numerical calculation of mie theory," *J. Appl. Opt.*, vol. 28, no. 3, pp. 363–366, 2007.

[48] Y. Shih and F. G. Shi, "Quantum dot based enhancement or elimination of color filters for liquid crystal display," *IEEE J. Sel. Topics Quantum Electron.*, vol. 23, no. 5, Sep./Oct. 2017, Art. no. 1901304.

[49] S. Lin *et al.*, "Multi-primary-color quantum-dot down-converting films for display applications," *Opt. Exp.*, vol. 27, no. 20, pp. 28480–28493, 2019.

[50] H.-J. Kim, M.-H. Shin, and Y.-J. Kim, "Optical efficiency enhancement in white organic light-emitting diode display with high color gamut using patterned quantum dot film and long pass filter," *Japanese J. Appl. Phys.*, vol. 55, no. 8S3, 2016, Art. no. 08RF01.

[51] X. H. Wang, P. T. Lai, and H. W. Choi, "The contribution of sidewall light extraction to efficiencies of polygonal light-emitting diodes shaped with laser micromachining," *J. Appl. Phys.*, vol. 108, no. 2, Art. no 023110, 2010.

[52] Y. Chu, M. Wu, C. Chung, Y. Fang, and Y. Su, "Micro-chip shaping for luminance enhancement of GaN micro-light-emitting diodes array," *IEEE Electron Device Lett.*, vol. 35, no. 7, pp. 771–773, Jul. 2014.

[53] T. A. Savas, M. L. Schattenburg, J. M. Carter, and H. I. Smith, "Large-area achromatic interferometric lithography for 100 nm period gratings and grids," *J. Vac. Sci. Technol. B: Microelectronics Nanometer Structures Process., Meas., Phenomena*, vol. 14, no. 6, pp. 4167–4170, 1996.

[54] C. Ru, J. Luo, S. Xie, and Y. Sun, "A review of non-contact micro- and nano-printing technologies," *J. Micromechanics Microengineering*, vol. 24, no. 5, 2014, Art. no. 053001.